


Article

Influence of Oil Injection Lubrication Parameters of High-Speed Internal Meshing Gear Based on the Computational Fluid Dynamics

Peixun Tang ^{1,2}, Zhengminqing Li ^{1,2,*}, Xiangying Hou ^{1,2} , Letian Li ^{1,2}, Rongsheng Xi ^{1,2} and Yiyang Chen ^{1,2}

¹ College of Mechanical and Electrical Engineering, Nanjing University of Aeronautics and Astronautics, Nanjing 210016, China; ptang@tcd.ie (P.T.); houxiangying@126.com (X.H.); liletian200@nuaa.edu.cn (L.L.); xirongsheng930@163.com (R.X.); yiyanchen2022@163.com (Y.C.)

² National Key Laboratory of Helicopter Aeromechanics, Nanjing University of Aeronautics and Astronautics, Nanjing 210016, China

* Correspondence: lzmq_cmee@nuaa.edu.cn

Abstract: High-speed gears are crucial transmission components found in airplanes and other systems, and they are maintained primarily through oil injection. However, due to their high operating speeds and the influence of oil injection settings, gear surface lubrication efficacy is frequently insufficient, compromising the transmission system's precision, durability, and safety. Currently, the parameter choices for oil injection in high-speed gears mostly rely on empirical judgment, which results in significant time and resource expenses. This study focuses on one pair of internal meshing gears within a specific aircraft gearbox, establishing an oil injection lubrication model for high-speed internal meshing gears using the computational fluid dynamics (CFD) approach. This research provides insights and references for optimizing oil injection parameters and improving lubrication efficiency in high-speed internal meshing gear systems by examining the dynamic characteristics of internal meshing wind resistance in addition to the effects of injection tube position, angle, and speed on lubrication performance.

Keywords: aero gearbox; oil spray lubrication; internal meshing gear; gear transmission



Citation: Tang, P.; Li, Z.; Hou, X.; Li, L.; Xi, R.; Chen, Y. Influence of Oil Injection Lubrication Parameters of High-Speed Internal Meshing Gear Based on the Computational Fluid Dynamics. *Lubricants* **2024**, *12*, 390. <https://doi.org/10.3390/lubricants12110390>

Received: 8 October 2024

Revised: 31 October 2024

Accepted: 11 November 2024

Published: 13 November 2024



Copyright: © 2024 by the authors. Licensee MDPI, Basel, Switzerland. This article is an open access article distributed under the terms and conditions of the Creative Commons Attribution (CC BY) license (<https://creativecommons.org/licenses/by/4.0/>).

1. Introduction

High-speed gears are widely used in vehicles, aircrafts, and other essential areas because of their high transmission accuracy, consistent transmission ratio, smooth transmission, and high efficiency [1]. Oil injection lubrication, being one of the primary lubrication systems for high-speed gears, has an impact on gear life and transmission efficiency. However, due to the high speed of high-speed gears, their complex operating circumstances and injection pipe settings are primarily determined through experience and other factors, resulting in poor high-speed gear lubrication, vibration or damage in bearings and other components, and even major accidents [2–4]. Many researchers have investigated or applied computational fluid dynamics (CFD) methodologies to problems such as gear injection lubrication in order to reduce computational time and cost.

In the 1970s and 1980s, Akin et al. researched gear oil injection lubrication and completed many sets of experimental tests to research the impact of fuel injection design parameters and gear characteristics on the fuel injection effect [5–7]. In 2009, Arisawa et al. used the computational fluid dynamics (CFD) approach of an oil/air two-phase flow for the first time to examine gear drag and mixing loss, demonstrating that the method is an excellent tool for studying high-speed gear drag loss [8]. Diab et al. proposed two theoretical methods for high line velocity drag: (1) dimensional analysis and (2) fluid flow around a rotating gear [9]. Sylvain pallas et al. used a computational fluid dynamics (CFD) program to study the wind power loss of spur gears while rotating in pure air. The gear

drive flow field motion track diagram is shown in Figure 1 [10]. Fondelli et al. employed the computational fluid dynamics (CFD) method to analyze the oil injection loss, using the volume of fluid method (VOF) approach to numerically study the influence of a single oil jet on a single high-speed gear [11]. In 2020, Hurrell conducted a study on power losses in gear oil spray lubrication with shrouds. Computational fluid dynamics (CFD) simulations confirmed the advantages of the optimal shroud design in reducing power loss. Additionally, the simulations revealed a significant axial component in the oil flow at the meshing point, supporting the rationale for providing openings in the optimal shroud structure [12]. Li et al. employed a computational fluid dynamics (CFD) numerical model to analyze the fluid distribution, velocity field, and pressure field surrounding the gear during oil injection lubrication and determined the mechanical and energy properties of gear clearance power loss [13]. Wang et al. used CFD to explore the effects of injection angle and injection position parameters on the lubrication effect and suggested potential nozzle parameter design methods when applying oil injection lubrication [14,15]. Jiang et al. recommended a high-speed-gear oil injection heat-dissipation model, based on the CFD method, adopted the static heat flow coupling technique to study the gear heat dissipation issue, and predicted the influence of optimal oil injection lubrication angle and distance on cooling through the regression orthogonal method [16]. Mo et al. discussed and examined two oil injection methods for asymmetric helical gears. The effects of gear speed and spray velocity on the oil volume fraction and pressure were examined using the computational fluid dynamic (CFD) approach to establish a lubrication model of asymmetric helical gears. Figure 2 depicts an oil injection diagram for two types of gear [17]. Zhu et al. conducted a detailed study on the oil injection lubrication properties of spiral bevel gears and modified critical position parameters such as the nozzle position, injection elevation angle, and angle of the azimuth utilizing mathematical modeling and CFD methods [18–20].

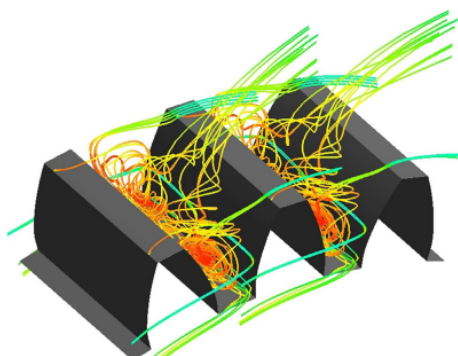


Figure 1. Gear drive flow-field motion track diagram [10].

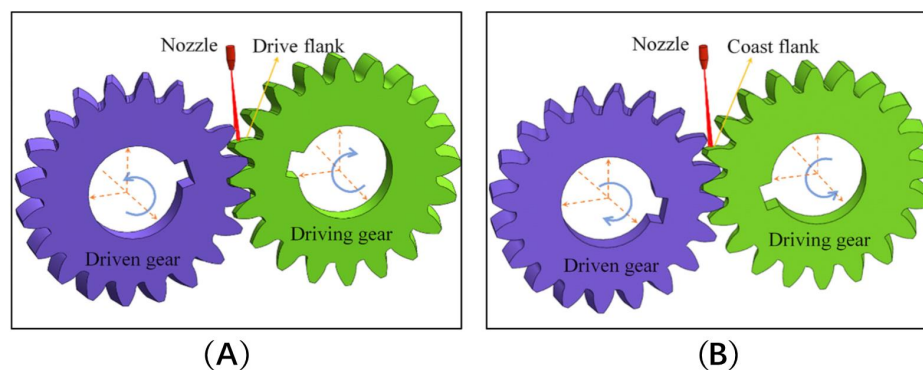


Figure 2. Coast flank injection lubrication method and drive flank injection lubrication method: ((A) coast flank oil injection; (B) drive flank oil injection) [17].

Wei et al. used the CFD method to explore the influence of airflow on the lubrication effect of a variable hyperbolic circular-arc-tooth gear in the form of oil injection lubrication,

determined the best oil injection angle, and provided a theoretical optimization of the design and parameters of the oil injection lubrication system and the cooling system of the gear transmission [21].

The Volume of Fluid (VOF) model is an essential model used in this research. The model mimics two or three immiscible fluids by solving separate momentum equations and accounting for the volume of each fluid that passes through the region. Most of the aforementioned gear lubrication research used the VOF model, which simulates the violent interaction between oil injection and air created by the rotating gear during the gear injection lubrication process [22,23]. The VOF method proposed by Hirt and Nichols is one of the most suitable methods to simulate the impact of an oil jet on moving gear teeth [22]. Crouchez and Morvan proposed a similar VOF calculation using the adaptive mesh method to simulate the lubricating oil's behavior in the bearing chamber of an aero-engine. The advantages and disadvantages of the fixed grid method and the adaptive grid method were compared. It was found that the VOF simulation using the adaptive grid method has better robustness and stability, and has advantages in terms of runtime acceleration [24].

In conclusion, previous research focuses on the use of oil injection lubrication for external meshing gears, focusing on the wind resistance movement characteristics of the external meshing gear as well as the design of important parameters, such as the oil injection angle in the design of the oil injection lubrication, and provides conclusions and relevant rules. However, studies on the lubricating properties of internal meshing gears are limited. Furthermore, the motion characteristics of the internal meshing gear and the injection pipe are distinct from the oil injection lubrication of the external meshing gear.

This study investigates a pair of simplified high-speed internal meshing gears, their wind-resistance motion trajectories, and the effect of injection parameters on the lubrication of the internal meshing gears. The computational fluid dynamics model of the gear was generated using computational fluid dynamics software 2022R1 with excellent precision and stability based on the VOF model, K-epsilon turbulence model, and dynamic mesh model. This research investigates the properties of air movements around the gear in non-lubricating situations; additionally, the effects of injection device position parameters, injection angle, and injection speed on internal gear lubrication are examined, serving as a reference for the oil injection lubrication design of high-speed internal meshing gears.

2. Materials and Methods

2.1. Mathematical Model of Multiphase Model (VOF)

Ansys' fluent module comprises the Volume of Fluid (VOF) model, the mixture model (mixture), and the Euler model. This research discusses two immiscible fluids (air and lubricating oil) and uses the Volume of Fluid (VOF) model to analyze the impact of lubrication based on oil distribution.

2.1.1. Phase Volume Fraction Calculation Model

The formula of the phase volume fraction calculation is shown here, where N is the number of fluid phases, φ_1 represents the physical parameters of the fluid, and r_1 represents the volume fraction, total integral number and 1. Because, in this article, two kinds of fluid (air and oil) are required, $r_1 + r_2 = 1$.

$$\sum_{i=1}^N = r_1 \varphi_1 \quad (1)$$

2.1.2. Multiphase Model (VOF) Momentum Equation

The VOF momentum equation combines the fluid density (ρ); velocity (u); pressure (p); viscosity (μ); temperature (T); gravitational acceleration (g); and surface tension (F).

$$\rho \frac{\partial u}{\partial t} + \cdot \nabla (\rho u u) = -\nabla p + \nabla \cdot \left(\mu \left(\nabla u + \nabla u^T \right) \right) + p g + F \quad (2)$$

2.1.3. Multiphase Model (VOF) Energy Equation

$$\frac{\partial}{\partial t}(\rho E) + \nabla \cdot V(\rho E + p) = \nabla \cdot (k \nabla T) + Q \quad (3)$$

In this formula, ρ is the fluid density; E is the total energy; k is the thermal conductivity coefficient; T is the temperature; Q is the energy source.

2.2. Turbulence Model

Because the K-epsilon model is widely used, and given the complexity of gear rotation and the issues with accuracy in the present investigation, this paper chose the K-epsilon model. The turbulent kinetic energy k and its dissipation rate were calculated using the transport equation presented below. The calculations in this article are based on the system's default settings. The formula is as follows:

$$\frac{\partial}{\partial t}(\rho \varepsilon) + \frac{\partial}{\partial x_i}(\rho \varepsilon u_i) = \frac{\partial}{\partial x_j} \left[(\mu_a A_\lambda) \frac{\partial \varepsilon}{\partial x_j} \right] + C_{1\lambda} \frac{\varepsilon}{k} (G_k + C_{3\lambda} G_b) - C_{2\lambda} \rho \frac{\varepsilon^2}{k} + S_\varepsilon \quad (4)$$

In this formula, G_k turbulent kinetic energy is created for the average velocity gradient; G_b is produced by the buoyancy turbulence kinetic energy; $C_{1\lambda}$, $C_{2\lambda}$, and $C_{3\lambda}$ are constants.

2.3. Dynamic Mesh Technology

Furthermore, dynamic mesh technology is a key technology in this study. This study defines gear motion using dynamic grid technology and user-defined UDF function. To achieve the iteration of the governing equation under the motion state of the dynamic grid, some mesh nodes with a high degree of spatial distortion must be reconfigured, and the quality of the local rebuilt mesh is enhanced by employing the re-mesh and smoothing techniques. The conservation equation of dynamic mesh can be written as follows:

$$\frac{d}{dt} \int_{V_h} \rho \beta dV_h + \int_{\partial V_h} \rho \beta (u_i - u_m) \cdot dA_i = \int_{\partial V_h} \Gamma \beta \cdot dA_i + \int_V S_g dV_h \quad (5)$$

where V_h is the control volume, whose form and size change over time; u_m is the velocity of the grid motion; ρ represents the fluid density; Γ represents the dissipation coefficient; the source term for scalar β is S_g .

The derivative term in Equation (5) is determined as follows:

$$\frac{d}{dt} \int_{V_h} \rho \beta dV_h = \frac{(\rho \beta V_h)^{n+1} - (\rho \beta V_h)^n}{\Delta T} \quad (6)$$

The following formula is used to calculate the control volume V_h^{n+1} for the $(n + 1)$ time step:

$$V_h^{n+1} = V_h^n + \frac{dV_h}{dt} \Delta T \quad (7)$$

where $\frac{dV_h}{dt}$ represents the control volume's time derivative. In order to satisfy the grid conservation law, the derivative of the control volume with respect to time is calculated as follows:

$$\frac{dV_h}{dt} = \int_{\partial V_h} u_m \cdot dA_i = \sum_j^n u_{m,j} \cdot A_j \quad (8)$$

where, the number above the control volume is denoted by n , and the surface's area vector is A_j .

2.4. Computational Domains

This study is based on the internal meshing gear transmission system in the transmission mechanism of an aircraft, and its overall structure diagram is shown in Figure 3.

To facilitate the study of the calculation domain in the internal meshing gearbox, the internal meshing gearbox needs to be simplified, as shown in the simplified calculation domain of the internal meshing gearbox system in Figure 4. Tables 1 and 2 also indicate multiple features of the internal fluid field in the gearbox, as well as the internal meshing gear parameters.

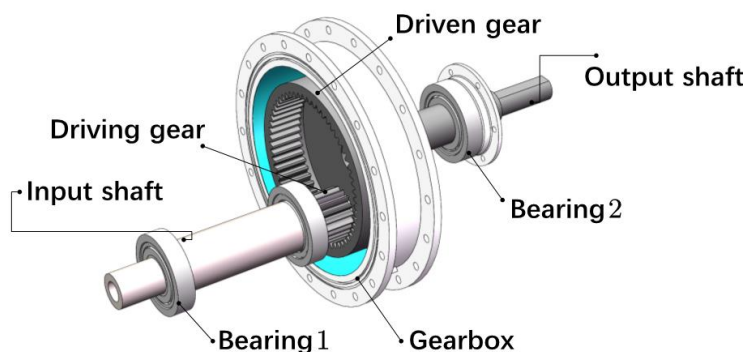


Figure 3. Internal meshing gear transmission structure of an aircraft type.

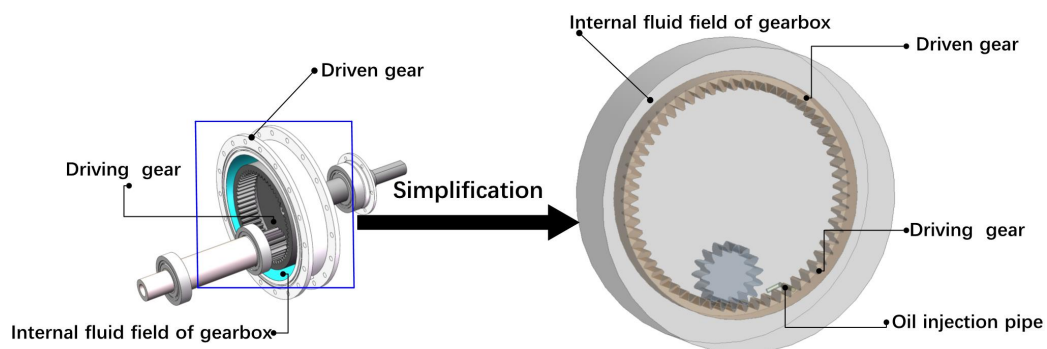


Figure 4. Simplified diagram of the calculation domain of internal fluid field gearbox.

Table 1. The parameters of internal fluid field in the gearbox.

Parameter	Gear Box
Diameter (mm)	406
Height (mm)	55
Nozzle diameter (mm)	2
Initial oil injection velocity (m/s)	40

Table 2. The parameters of the internal meshing gear.

Parameter	Driving Gear	Driven Gear
Number of teeth	15	59
Modulus (mm)	2.5	2.5
Pressure angle	22.5°	22.5°
Tooth width (mm)	35	33
Center distance (mm)	54	54
Gear linear velocity (m/s)	17.37	17.37

2.5. Meshing of Computational Domains

Unstructured tetrahedral meshing was used to generate the mesh for the internal meshing gears, ring gear, oil injection system, and the simplified gearbox calculation domain. To balance accuracy and computational efficiency, the element size was set to 3 mm. Curvature and proximity capture were enabled, with the curvature proximity value set to 0.3. The average mesh quality was greater than 0.8, indicating a high-quality mesh.

The total number of mesh elements was 3,524,457. A cross-section diagram of the result of the grid division is shown in Figure 5.

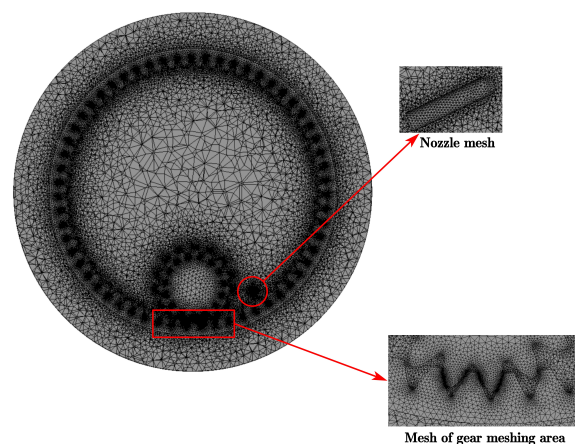


Figure 5. The cross-section diagram of the result of mesh division.

2.6. Boundary Condition Setting

The transient approach was used to identify the fluid calculation domain. The gravity effect is considered by selecting the gravity option and entering a value of 9.8 m/s^2 . Because the internal flow field of the gearbox is primarily composed of oil and air, the physical properties of the oil and air must be selected using the fluid option. The physical characteristics of air were obtained using the software's default mode, and the oil was aviation lubricating oil, grade 4106. The basic physical specifications of this oil are listed in Table 3. In order to regulate the boundary parameter variables and assure the comparability of the experimental findings, a lubricating oil viscosity of $56.46 \text{ mm}^2/\text{s}$ was used universally in this investigation. The transmission speed and direction of the gear system were set using the user-defined function (UDF). The intake injection speed was determined using the boundary condition settings. To guarantee the convergence and accuracy of the computation, the SIMPLE method was used for the pressure–velocity coupling solution, the pressure term was discretized using the PRESTO format, and the calculation time step was set to $1 \times 10^{-6} \text{ s}$.

Table 3. The basic parameters of aviation 4106 oil.

Parameter	Temperature	Aviation 4106 Oil
Kinematic viscosity (mm^2/s^2)	40 °C	24.40
	−40 °C	8652
	100 °C	5.02
Flash point (°C)		250
Pour point (°C)		<−54
Evaporation loss (%)	(204 °C, 6.5 h)	4.37

3. Results and Discussion

This study investigated the airflow conditions of high-speed internal meshing gears (with only the gears rotating and no oil being injected) by analyzing the air velocity contour diagram and trace diagram. The oil injection trajectory in the gearbox cross-section, the distribution of oil on the gear and the ring gear, and the average oil volume fraction under different oil injection parameters were analyzed. Comparing the lubricating qualities of various parameters provides a reference for identifying the best injection parameters and offers useful insights into the design of injection systems in high-speed internal gear applications.

3.1. Air Movement Characteristics Under Gear Rotation (No Injection Lubrication)

Figure 6 shows the airflow characteristics near the internal gear within the gearbox cross-section, as well as the airflow trajectory near the gear during rotation (gear rotation only, without oil injection). Figure 6a primarily serves to present the range of air velocity near the gears. The phase diagram reveals that the overall air velocity at the meshing inlet is greater than that at the meshing outlet, with air velocities at the meshing inlet ranging from approximately 13 to 17 m/s, and at the meshing outlet ranging from 8 to 14 m/s. Additionally, it can be observed that the air velocity caused by the gears is greater than that caused by the ring gear, due to the gears' speed being higher than that of the ring gear. Figure 6b depicts the air velocity trajectory near the gear during rotation, where the air velocity at the meshing inlet of the gears and the ring gear is higher than in other areas. One of the main reasons for this phenomenon is that the internally meshing gears move in the same direction. The rapid speed of the driving wheel causes the air velocity to diffuse into the surrounding area. Furthermore, the flow velocity trajectories at the meshing outlet are more chaotic than those at the meshing inlet.

The above research mainly aims to provide an analysis of the air motion characteristics of internal meshing gear, which is helpful in understanding the motion characteristics of internal meshing gears.

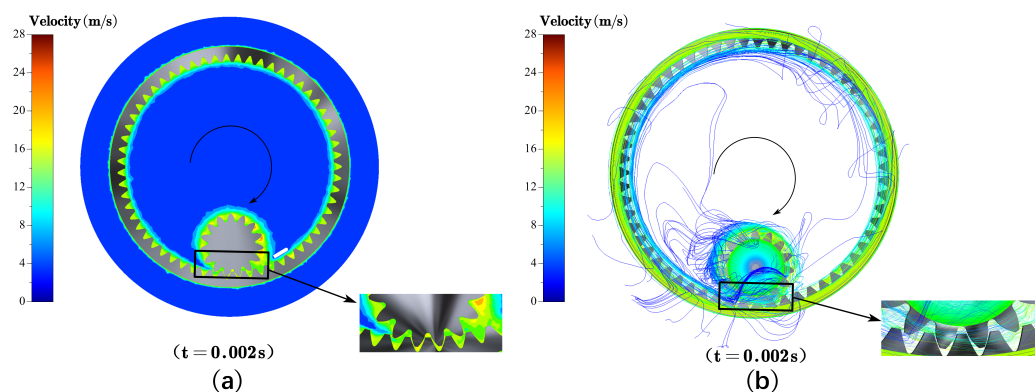


Figure 6. Diagram of the airflow resistance characteristics near the gear during its motion. ((a) Contour figure of air velocity under gear rotation; (b) diagram of air velocity trace under gear rotation).

3.2. Influence of Nozzle Position Parameters on Lubrication of Internal Meshing Gear

The impact of position factors on internal gear lubrication was investigated by adjusting the longitudinal position of the oil injection port based on its initial position. A maximum of three places were developed, with a 1 mm spacing between then injection positions, for which a schematic diagram is presented in Figure 7. This section examines the injection trajectory in the gear box's cross-section, the distribution of oil on the gear and ring gear, and the average oil volume fraction under various injection parameters to demonstrate the effect of injection position parameters on internal meshing gear lubrication.

Figure 8 presents a cross-sectional view of the gearbox, showing the trajectory and distribution of the lubricant at 0.002 s as it is injected into the gears. It is possible to assess the influence of nozzle location on the lubrication performance of the gear system by monitoring the lubricant's route and volume fraction fluctuations (with brighter colors indicating greater lubricant concentrations). When comparing Position 1 to the initial position, the overall lubricant volume fraction in Position 1 during injection into the meshing zone is noticeably brighter and higher lubricant at the meshing entry. Position 2 has the brightest color for the oil volume fraction along the path from oil injection to the meshing zone. However, Position 2 is too close to the ring gear, causing a high oil volume distribution in other parts of the gear meshing zone. The overall oil volume percentage of the oil path at position 3 is lower than that at the initial position. It is worth noting that the oil distribution in the red area at position 3 is wider than that in the initial position and

position 2. However, position 3 has a deeper color for the total oil volume proportion in the red zone than position 1.

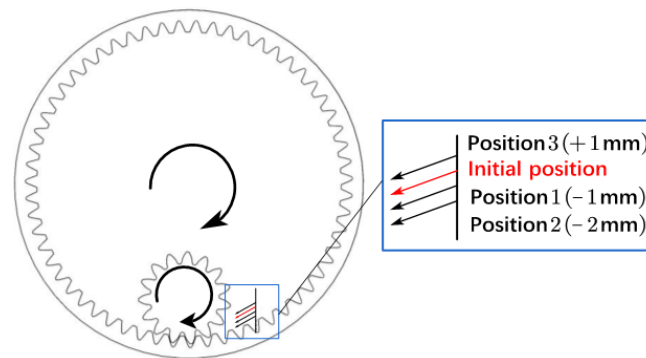


Figure 7. Schematic diagram of the influence of injection position parameters on the lubrication of the internal meshing gear (each arrow indicates the center line of the oil injection port, with the red arrow representing the center line of the oil injection port's initial location).

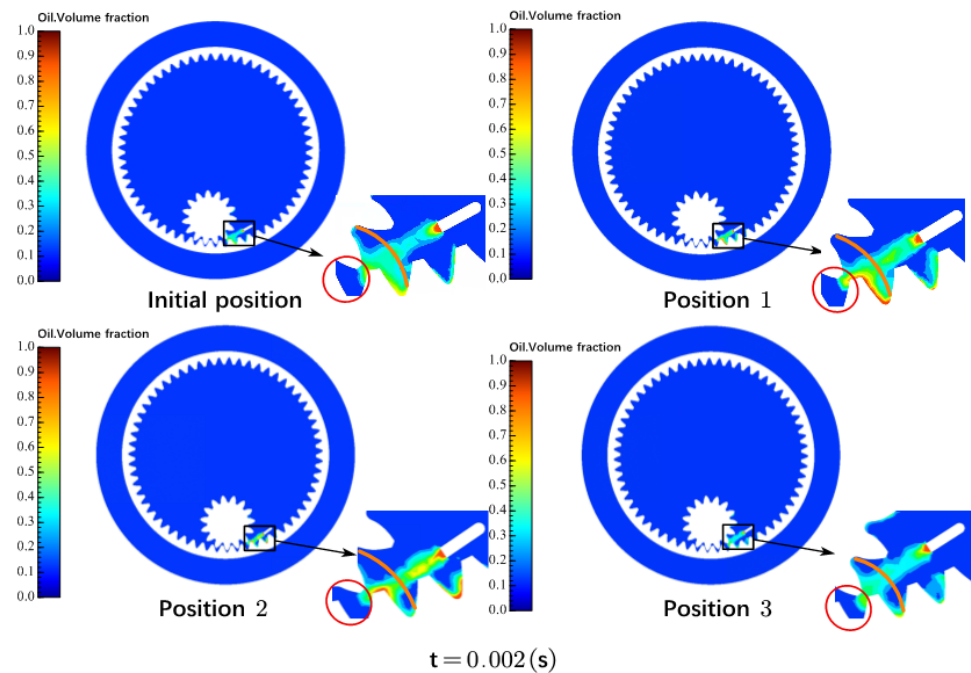


Figure 8. The oil injection trajectory in the gearbox cross-section for different positions: ((1) the red region indicates where the gear and ring gear will be joined; (2) the closed region, represented in orange, and the gear surface comprise the meshing intake area).

Figure 9 shows the lubricant distribution and volume fraction for the gear. By comparing the four places, it is clear that the oil distribution in other sections of the gear diminishes due to the fact that the impact of oil distribution on the gear decreases as the oil injection port moves away from it. Additionally, at Position 3, the lubricant distribution in the meshing zone is the most extensive. Figure 10 shows the distribution and volume of the lubricating oil on the ring gear. When the nozzle is set to position 1, the area with the highest percentage of lubricating oil volume in the engagement area is the brightest. However, as the injection position approaches the ring gear, the color of the oil volume fraction in the meshing area darkens, whilst the color of the oil volume fraction in other places brightens. This is caused by the gravity of the oil and the nozzle being too close to the ring gear.

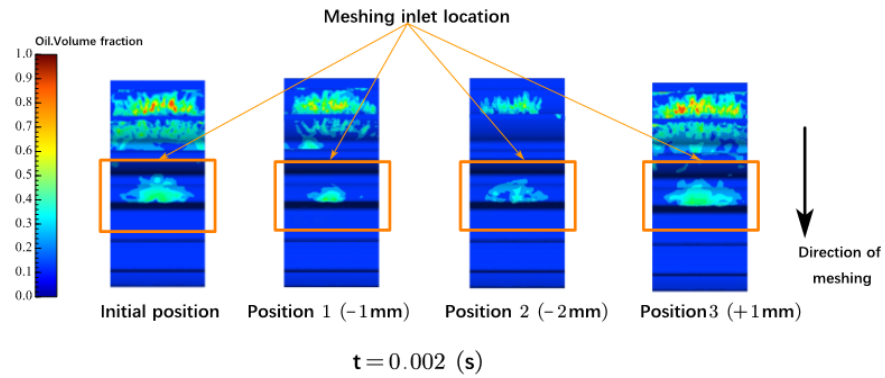


Figure 9. Distribution of the gear-lubricating fluid in four different position parameters (the orange region represents the meshing intake area).

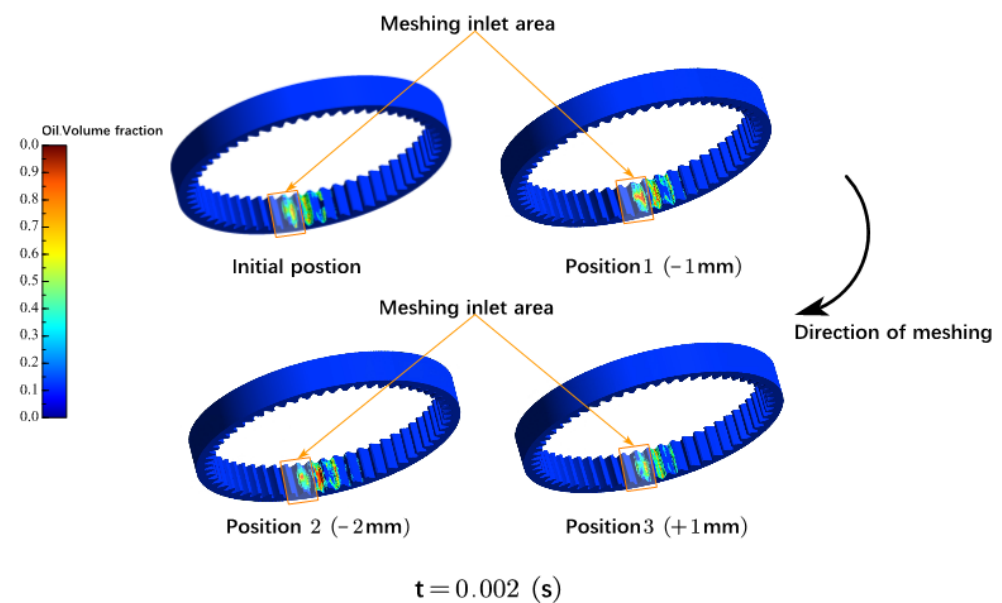


Figure 10. Distribution of lubricating fluid across ring gears under four distinct position conditions (the orange region represents the meshing intake area).

Figure 11A depicts a comparison of the average oil volume fractions at the mesh of gears and ring gear surfaces for different injection positions (orange area). As the oil injection port advances closer to the ring gear, the oil volume fraction increases, with the greatest value of 0.2492 being obtained for Position 1, representing a 23.9% increase over the initial position. When the nozzle continues to deflect to the ring gear and reaches Position 2, the oil volume fraction is 0.181, a 27.3% drop from Position 1. Figure 11B shows the average oil volume distribution on the ring gear and gear surfaces in the red area of Figure 8. It can be seen that when the oil injection port moves closer to the ring gear, the highest value of the average oil volume fraction is found at position 1, which is 0.056, 24.4% greater than that at the initial position. However, as the injection location shifts to position 2, the average oil volume percentage reduces by 21.4%. In Position 3, while the average oil volume percentage in the orange zone is lower than the initial position, it is larger in the red region, with a value of 0.049.

According to the findings, Position 1 has the best overall lubricating effect. Moving the nozzle in the direction of the ring gear (low speed) improves the lubricating action, but avoids getting too near.

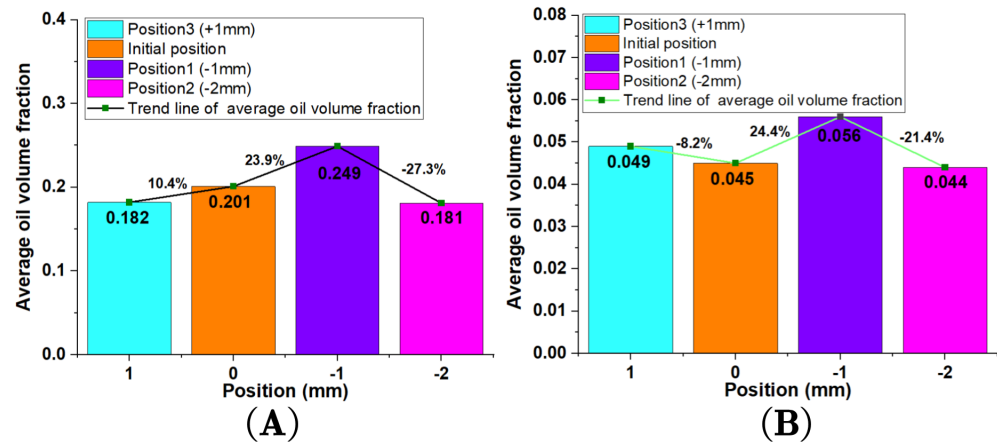


Figure 11. The average oil volume fraction at the meshing inlet area: (Figure (A) depicts the average oil volume fraction on the gear surfaces in the orange zone; Figure (B) depicts the average oil volume fraction on the gear surfaces in the red zone).

3.3. Influence of Nozzle Angular Parameters on Lubrication of Internal Meshing Gear

The influence of the angle factor on the lubrication of the internal gear is examined by modifying the angle of the oil injection port based on the initial position, and the maximum three angle settings are produced, each angle is 2° apart. The schematic diagram is depicted in Figure 12. This part investigates the injection trajectory in the gear box’s cross section, the oil distribution on the gear and ring gear, and the average oil volume fraction under different injection parameters to show how injection angle parameters affect internal meshing gear lubrication.

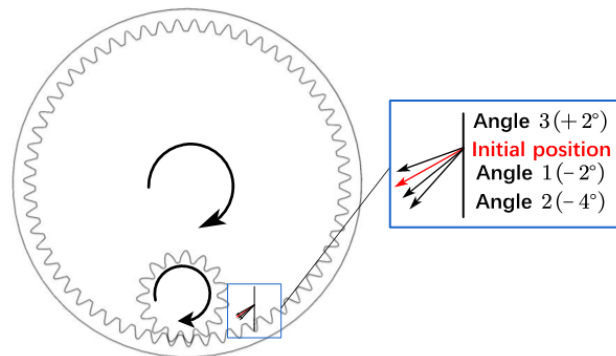


Figure 12. Schematic diagram of the influence of injection angular parameters on the lubrication of internal meshing gear (Each arrow indicates the center line of the oil injection port, with the red arrow representing the center line of the oil injection port’s initial position).

Figure 13 provides a cross-sectional view of the gearbox, illustrating the changes in oil volume fraction and the trajectory of the oil movement during the injection process at 0.002 s. Analyzing the oil trajectory and volume fraction color changes in Figure 13 can allow for an evaluation of the influence oil injection angle’s influence on the lubrication performance of the gear system. This analysis offers valuable insights into how the injection angle affects gear lubrication. Comparing the four angles, it is clear that when the oil injection angle points away from the gear, the oil volume fraction deepens along the route to the gear meshing inlet. The brightest overall oil volume fraction was obtained at Angle 2, but Angle 2 leads to a lower volume of oil in the gear meshing zone (red zone) compared to Angle 3 and its initial position. Furthermore, Angle 1 leads to a greater percentage of oil volume when compared to the oil distribution color in the meshing intake region at the initial position, and also has a higher oil dispersion in the gearing area than Angle 2.

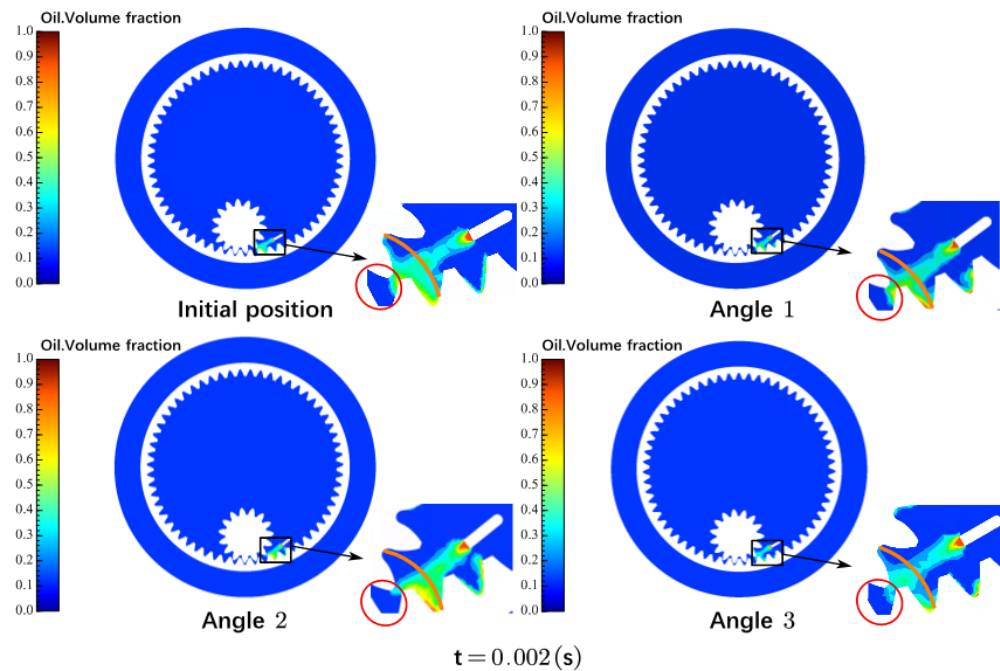


Figure 13. The figure of oil injection trajectory in a gearbox cross-section under different angles: ((1) the red region indicates where the gear and ring gear will be joined; (2) the closed region produced by the orange area and gear surface represents the meshing intake area).

From the analysis of Figure 14, comparing the oil distribution at the initial position with that at Angle 3 on the gear, it is evident that the oil volume fraction at the gear meshing area is brighter in color at the initial position than at Angle 3. This indicates that when the nozzle angle also approaches the gear (at higher rotational speeds), it has a negative impact on lubrication effectiveness. Additionally, as the oil injection angle shifts toward the ring gear, the oil distribution on the gear gradually decreases, reaching its minimum at the gear meshing area when the oil injection angle changes to Angle 2.

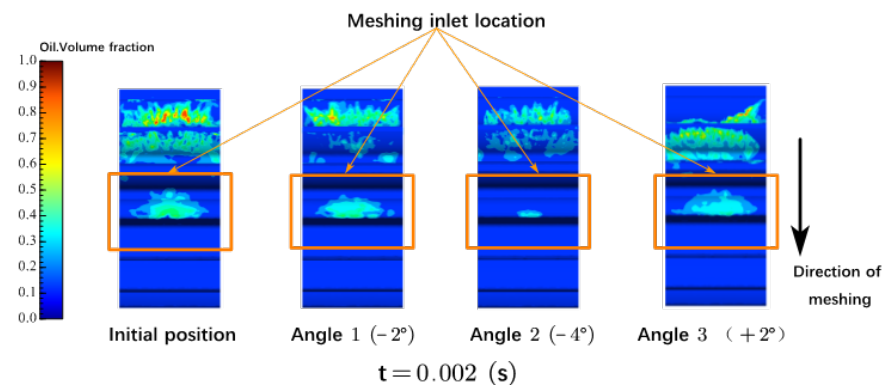


Figure 14. Distribution of gear-lubricating fluid under four diverse angular parameters (the orange region represents the meshing intake area).

By analyzing Figure 15, it can be observed that as the angle shifts toward the ring gear, the color distribution of the oil on the ring gear becomes brighter, and the oil distribution across other parts of the ring gear at the meshing area becomes more extensive. However, at Angle 2, the oil distribution across the other areas of the ring gear is the most widespread. The oil distribution and total oil volume percentage in Angle 2's ring gear meshing area are less than those in Angle 1 due to the oil's gravity and the oil injection port's proximity to the ring gear.

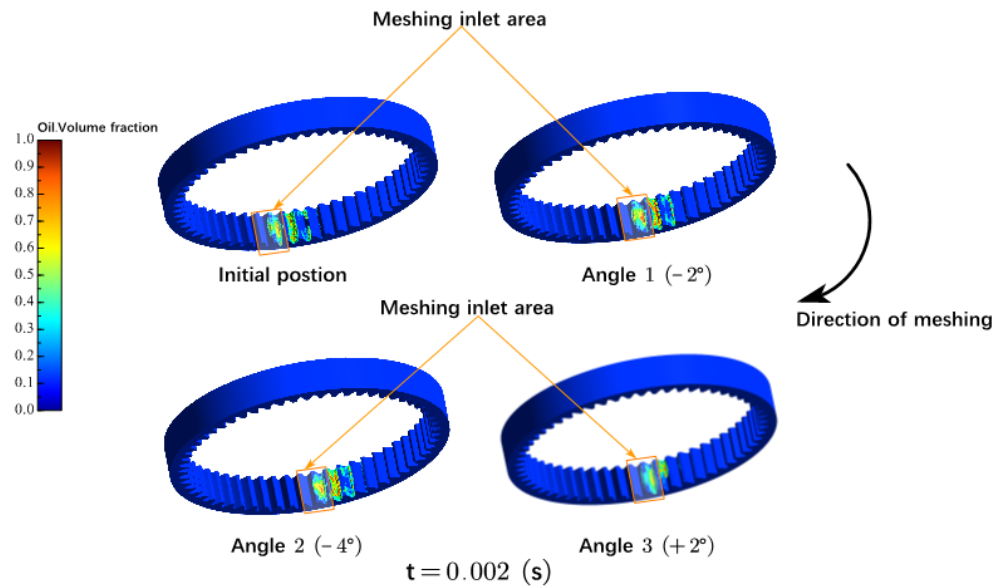


Figure 15. Distribution of lubricating fluid across the ring gears under four different angular conditions (the orange region represents the meshing intake area).

Figure 16A presents a comparison of the average oil volume fractions at the mesh of gear and ring gear surfaces at different injection angles (orange area). Through analysis, it can be observed that as the oil injection angle shifts from the gear to the ring gear, the oil volume fraction gradually increases, reaching a maximum value of 0.229 at Angle 1, an 13.9% increase compared to the initial position. However, as the angle continues to shift toward the ring gear, the oil volume fraction begins to decrease, with a 6.6% reduction at Angle 2 compared to Angle 1. Figure 16B shows the average oil volume distribution on the surfaces of the ring gear and the gear in the red area shown in Figure 13. Through comparison, it can be seen that the average oil volume percentage in the red region follows a tendency of first growing and then dropping, which is quite similar to the trend in Figure 16A. For Angle 1, the gear surfaces in the red area have the highest average oil volume fraction, which is 0.048. Angle 1 is deflected to Angle 2, which has the lowest average oil volume percentage, 0.02, showing a 58.3% drop compared to Angle 1.

This research demonstrates that Angle 1 has the best overall lubrication effect. To enhance the lubricating effect, the angle of the oil injection port was modified (leaning toward the ring gear), without approaching too near to it.

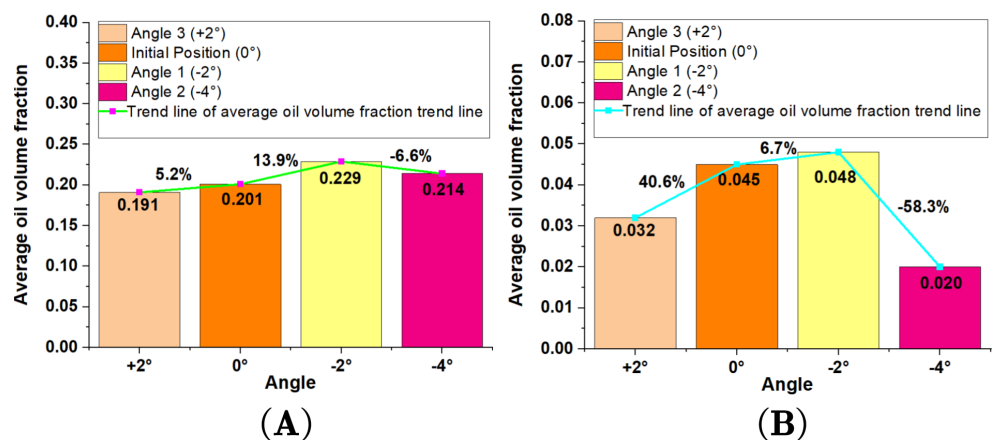


Figure 16. The average oil volume fraction at the meshing area (Figure (A) depicts the average oil volume fraction on the gear surfaces in the orange zone; Figure (B) depicts the average oil volume fraction on the gear surfaces in the red zone).

3.4. Influence of Oil Injection Speed Parameters on Lubrication of Internal Meshing Gear

Increases in the injection speed were used to investigate the effect of speed on internal gear lubrication based on the initial position and setting speed. Figure 17 depicts three alternative speeds, each of which is raised by 5 m/s. This section analyses the injection trajectory in the gear box's cross-section, the oil distribution on the gear and ring gear, and the average oil volume fraction under different injection parameters to show how injection speed parameters affect internal meshing gear lubrication.

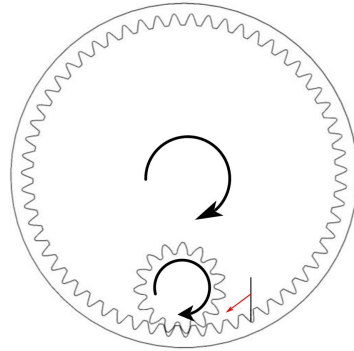


Figure 17. Schematic diagram of the influence of injection speed parameters on the lubrication of internal meshing gears (the red arrow represents the center line of the oil injection ports).

Figure 18 depicts a cross-section of the gear box and describes the change in oil volume fraction and oil movement trajectory during oil's injection into the gear at 0.002 s. By analyzing the oil trajectory and the color change for the volume fraction in Figure 18, the influence of oil injection speed on the lubrication effect of the gear system can be analyzed, providing a reference for the analysis of the influence of oil injection speed parameters on gear lubrication.

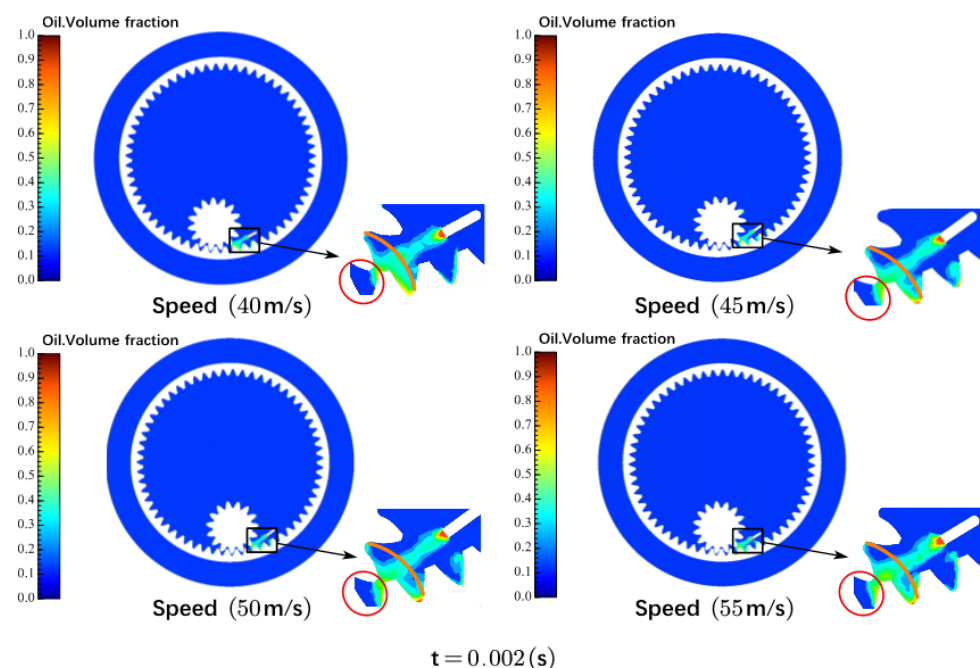


Figure 18. The oil injection trajectory in a gearbox cross-section under different speeds: ((1) the red region indicates where the gear and ring gear will be joined; (2) the closed region produced by the orange area and gear surface is the meshing intake area).

When different oil injection speeds are compared, it is discovered that as oil injection speed increases, the overall color of the oil trajectory in the area in which the oil is injected

into the gear meshing inlet becomes brighter. The oil is more widely distributed in the red area where the gear and ring gear are about to mesh (compared to the initial position). This is because the oil injection speed increases, causing the oil to enter the gear meshing region faster. At the same time, an intriguing occurrence can be observed: when the injection speed is raised from 45 m/s to 50 m/s, the color brightness and range of the oil volume portion in the red area increases by some amount. However, when the velocity is increased to 55 m/s, the brightness and range of the oil volume fraction in the red zone remain constant.

Figure 19 depicts the oil distribution and volume fraction on the gears. As the oil injection speed increases, more oil is delivered in the gear meshing region. However, when the oil injection speed increases to 55 m/s, the region with the highest oil volume fraction shrinks and the maximum oil volume fraction drops compared to that obtained under the oil injection speed of 50 m/s. This phenomenon may be explained by the fact that when the injection speed increases, the high oil velocity prevents efficient contact with the gear contact surface, resulting in a smaller oil volume fraction on the gear surface.

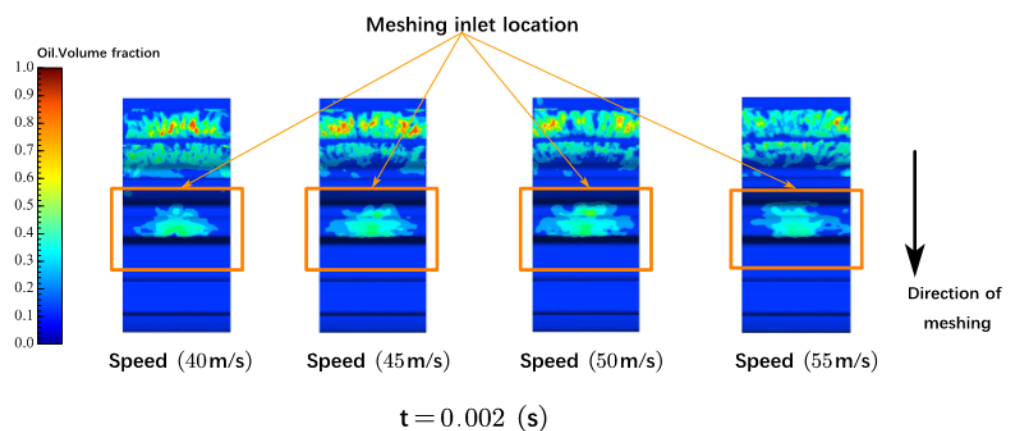


Figure 19. Distribution of gear-lubricating fluid under four different oil speed parameters (the orange region represents the meshing intake area).

Figure 20 depicts the oil distribution and volume percentage of the ring gear. As the oil injection speed increases, more oil is dispersed in the gear-meshing area, which is consistent with the gear's oil distribution. However, the analytical results for oil distribution on the gear differ in that the maximum oil volume fraction and range of oil volume fraction during meshing increase with speed, while the range of oil distribution in other parts of the ring gear meshing decreases. The causes of this condition are, on the one hand, the weight of the oil itself and on the other hand, the operation time of the oil, meaning that the oil speed is increased and the ring gear is longer owing to the consistency of the simulation time.

Figure 21A depicts a comparison of the average oil volume fractions at the mesh of gear and ring gear surfaces at different injection angles (orange area). The oil volume fraction increases with injection speed, reaching its maximum value of 0.253 at 55 m/s. Simultaneously, the growth rate of the oil volume portion increases. When the oil velocity ranges between 50 and 55 m/s, the oil volume fraction grows at the fastest rate, at 10.0%. Figure 16B illustrates the average oil volume distribution on the surfaces of the ring gear and gear in the red area of Figure 18. When the speed is increased to 50 m/s, the average oil-liquid integral value is at its highest, 0.062, but as the speed is gradually increased to 55 m/s, the average oil volume fraction decreases somewhat.

Based on previous studies, the overall best jet lubrication behavior occurs at a speed of 55 m/s (Figure 21A). However, the gear surface lubricating effect decreases slightly as one approaches the gear meshing area (Figure 21B). This demonstrates that increasing the injection speed is useful for improving the lubricating effect, but the speed should not be excessively high.

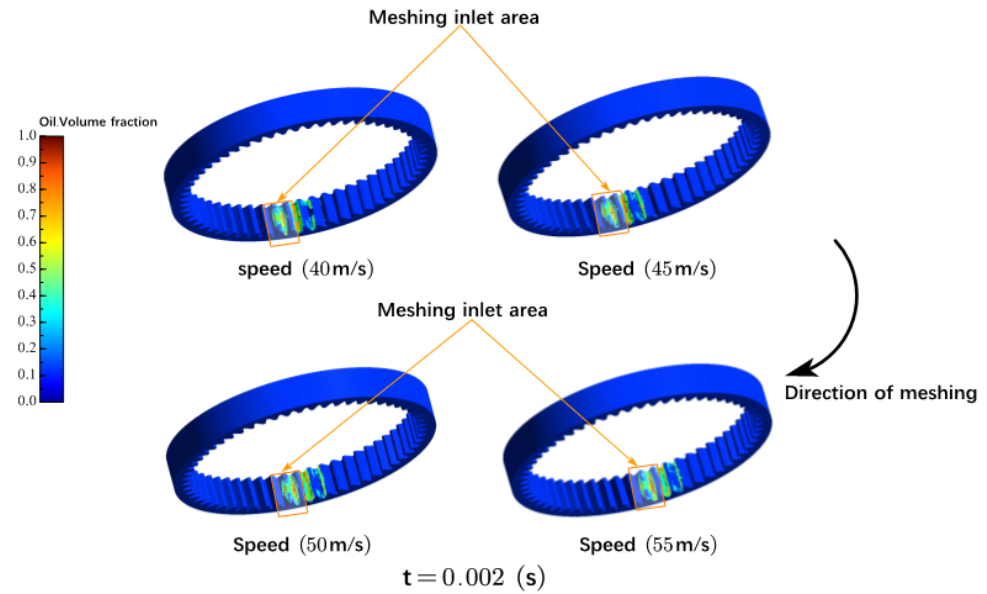


Figure 20. Distribution of lubricating fluid across ring gears under four different oil speed conditions (the orange region represents the meshing intake area).

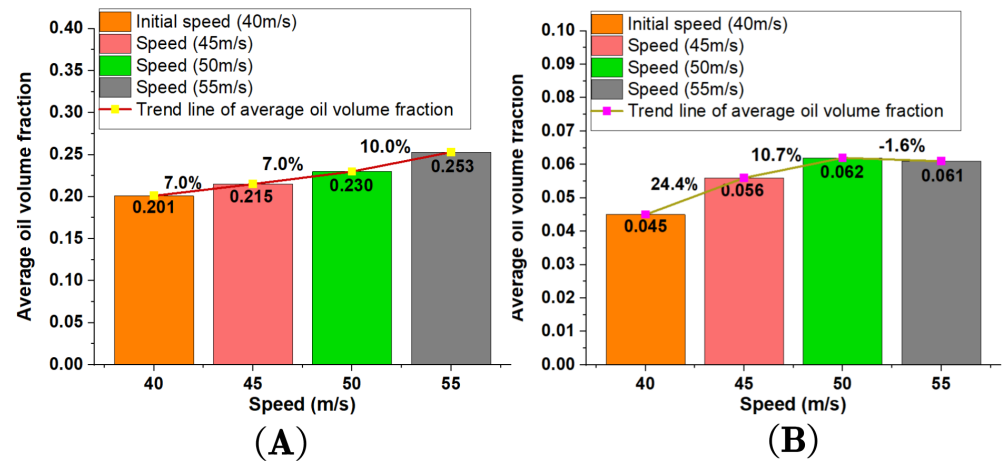


Figure 21. The average oil volume fraction in the meshing area: (Figure (A) depicts the average oil volume fraction on the gear surfaces in the orange area; Figure (B) depicts the average oil volume fraction on the gear surfaces in the red area).

4. Conclusions

This study utilized Computational Fluid Dynamics (CFD) to investigate the wind resistance characteristics of gears under non-lubricated conditions. It focuses on the effects of injection position, angle, and speed on the lubrication of high-speed internal meshing gears. The lubricating effects under various injection parameters are investigated, and design recommendations are made to improve the injection position parameters of the meshing inlet region of the high-speed internal meshing gear. The key findings are as follows:

1. This study provides an analysis of the airflow characteristics in high-speed internal meshing gears under non-lubricated conditions and examines the distribution and trajectory of air velocity within the gearbox. The overall velocity of air at the meshing intake is larger than the air speed at the meshing exit, which ranges between 13 and 17 m/s (simulation findings). Furthermore, the velocity trajectory at the meshing exit is less predictable than that at the meshing entrance. These findings can help to understand the motion characteristics of internal meshing gear under non-lubricated conditions.

2. The lubricating properties of internal meshing gear at various injection points are examined by this model. The findings indicate that moving the nozzle location to a specific range of ring gear can improve the lubricating effect. For instance, the maximum value of the average oil and volume values of the gear surface at the gear meshing inlet region is 0.249 (orange area) and 0.056 (red area), respectively, while the injection tube is at position 1. The average volume portion of the oil grew at the fastest rate, by 23.9% in the orange area and 24.4% in the red area. Excessive nozzle location relative to the ring gear will diminish the lubricating effect. For example, position 2 is 1 mm lower than position 1, resulting in a 27.3% decrease in average oil volume percentage when compared to position 1 (orange area).
3. The lubricating effect can be significantly improved by deflecting the nozzle angle in the direction of the ring gear at an acceptable angle. For example, in the simulation, lubrication is optimal when the deflection Angle is at Angle 1, and the average oil volume percentage is at its highest, with a red region of 0.048 and an orange region of 0.229. However, when the nozzle Angle is close to the gear ring, the oil's lubricating impact is reduced. For example, the average oil volume percentage of Angle position 2 in the orange area reduces by 6.6%, while the oil volume fraction in the red area decreases by 58.3%.
4. When the injection speed is increased from 40 m/s to 50 m/s, the oil distribution range on the gear surface increases and the average volume percentage of oil in the orange and red areas shows an upward trend. However, when the injection speed is too fast, the oil is unable to properly stay on the gear surface, resulting in poor lubrication. For example, when the injection speed increases from 50 m/s to 55 m/s, the average oil volume percentage in the orange area rises by 10.0%, whereas the average oil volume fraction in the red area falls by 1.6%. Furthermore, using bright colors on the gear surface tends to reduce the oil volume fraction area, as shown in Figure 19.

In conclusion, while the simulation period for internal meshing gear oil injection lubrication is brief and does not attain a steady state, the wind resistance characteristics under non-lubricating circumstances and the oil distribution for each injection parameter are consistent. As a result, this study may be used to build an internal meshing gear oil injection port and conduct a visual check of the gear box. It is advised that the steady-state circumstances be further assessed and the simulation analysis validated through experimentation.

Author Contributions: Conceptualization, P.T. and Z.L.; methodology, P.T.; software, P.T.; validation, P.T. and X.H.; formal analysis, P.T.; investigation, L.L.; resources, Z.L.; data curation, P.T.; writing—original draft preparation, P.T.; writing—review and editing, X.H. and Y.C.; visualization, R.X.; supervision, Z.L.; project administration, Z.L. All authors have read and agreed to the published version of the manuscript.

Funding: This research received no external funding.

Data Availability Statement: All the data are shown in the tables and figures of this paper.

Conflicts of Interest: The authors declare no conflicts of interest.

References

1. Lin, J.; Zhang, Z. Prospects of aeroengine power transmission system in the 21st century. *J. Aerosp. Power* **2001**, *16*, 108–114.
2. Wang, Y.Z.; Niu, W.T.; Tang, W.; Guo, M.; Li, G.Q. Influence of spray orientation parameters on spray lubrication process of aero spur gears. *J. Aerosp. Power* **2015**, *30*, 1605–1610.
3. Salunkhe, V.G.; Khot, S.M.; Jadhav, P.S.; Yelve, N.P.; Kumbhar, M.B. Experimental Investigation Using Robust Deep VMD-ICA and 1D-CNN for Condition Monitoring of Roller Element Bearing. *J. Comput. Inf. Sci. Eng.* **2024**, *24*, 124501. [[CrossRef](#)]
4. Salunkhe, V.G.; Desavale, R.G. An intelligent prediction for detecting bearing vibration characteristics using a machine learning model. *J. Nondestruct. Eval. Diagn. Progn. Eng. Syst.* **2021**, *4*, 031004. [[CrossRef](#)]
5. Akin, L.S.; Mross, J.J.; Townsend, D.P. Study of lubricant jet flow phenomena in spur gears. *J. Lubr. Tech.* **1975**, *97*, 283–288. [[CrossRef](#)]

6. Townsend, D.P.; Akin, L.S. Study of lubricant jet flow phenomena in spur gears—Out of mesh condition. *J. Mech. Des.* **1978**, *100*, 61–68. [[CrossRef](#)]
7. Akin, L.S.; Townsend, D.P. Into mesh lubrication of spur gears with arbitrary offset oil jet. Part 1: For jet velocity less than or equal to gear velocity. *J. Mech., Trans. Autom. Des.* **1983**, *105*, 713–718. [[CrossRef](#)]
8. Arisawa, H.; Nishimura, M.; Imai, H.; Goi, T. CFD simulation for reduction of oil churning loss and windage loss on aeroengine transmission gears. *Turbo Expo Power Land Sea Air* **2009**, 48821, 63–72.
9. Diab, Y.; Ville, F.; Velex, P.; Changenet, C. Windage losses in high speed gears—Preliminary experimental and theoretical results. *J. Mech. Des.* **2004**, *126*, 903–908. [[CrossRef](#)]
10. Pallas, S.; Marchesse, Y.; Changenet, C.; Ville, F.; Velex, P. A windage power loss model based on CFD study about the volumetric flow rate expelled by spur gears. *Mech. Ind.* **2012**, *13*, 317–323. [[CrossRef](#)]
11. Fondelli, T.; Andreini, A.; Soghe, R.D.; Facchini, B.; Cipolla, L. Numerical simulation of oil jet lubrication for high speed gears. *Int. J. Aerosp. Eng.* **2015**, *2015*, 752457. [[CrossRef](#)]
12. Hurrell, M.J. Shroud Effects on Load-Independent Power Loss of High-Speed Rotorcraft Gearing. Master’s Thesis, Cleveland State University, Cleveland, OH, USA, 2020.
13. Li, L.; Wang, S. Experimental study and numerical analysis on windage power loss characteristics of aviation spiral bevel gear with oil injection lubrication. *Stroj. Vestn.-J. Mech. Eng.* **2023**, *69*, 235–247. [[CrossRef](#)]
14. Wang, Y.Z.; Niu, W.T.; Wei, S.; Song, G.H. Influence of spin flow on lubricating oil jet: Design method of oil spray parameters to high-speed spur gears. *Tribol. Int.* **2015**, *92*, 290–300. [[CrossRef](#)]
15. Wang, Y.; Song, G.; Niu, W.; Chen, Y. Optimized design of spray parameters of oil jet lubricated spur gears. *Tribol. Int.* **2018**, *120*, 149–158. [[CrossRef](#)]
16. Jiang, X.; Zhou, C.; Su, J.; Jin, G.; Shen, R. Injection parameter design to improve the high-speed gear heat dissipation: CFD simulation and regression orthogonal experiment. *Simul. Model. Pract. Theory* **2023**, *128*, 102795. [[CrossRef](#)]
17. Mo, S.; Zou, Z.; Feng, Z.; Dang, H.; Gao, H.; Cao, X. Research on lubrication characteristics of asymmetric helical gear based on CFD method. *Lubr. Sci.* **2020**, *32*, 309–320. [[CrossRef](#)]
18. Zhu, X.; Dai, Y.; Ma, F. Development of a quasi-analytical model to predict the windage power losses of a spiral bevel gear. *Tribol. Int.* **2020**, *146*, 106258. [[CrossRef](#)]
19. Zhu, X.; Dai, Y.; Ma, F.; Ouyang, B. Mathematical modeling and numerical simulation for determining an optimized oil jet layout for spiral bevel gear lubrication. *Proc. Inst. Mech. Eng. Part J. Eng. Tribol.* **2021**, *235*, 611–628. [[CrossRef](#)]
20. Zhu, X.; Dai, Y.; Ma, F. On the estimation of the windage power losses of spiral bevel gears: An analytical model and CFD investigation. *Simul. Model. Pract. Theory* **2021**, *110*, 102334. [[CrossRef](#)]
21. Wei, Y.Q.; Yang, H.J.; Guo, R.; Liu, Y.P.; Dong, C.B. Analysis of Friction Characteristics and Transmission Efficiency of Gear with Variable Hyperbolic Circular-Arc-Tooth-Trace under Mixed Lubrication. *Tribology* **2024**, *44*, 1–12.
22. Hirt, C.W.; Nichols, B.D. Volume of fluid (VOF) method for the dynamics of free boundaries. *J. Comput. Phys.* **1981**, *39*, 201–225. [[CrossRef](#)]
23. Hu, X.; Li, P.; Quan, C.; Wang, J. CFD investigation on oil injection lubrication of meshing spur gears via lattice Boltzmann method. *Lubricants* **2022**, *10*, 184. [[CrossRef](#)]
24. Crouchez-Pillot, A.; Morvan, H.P. CFD simulation of an aeroengine bearing chamber using an enhanced volume of fluid (VOF) method: An evaluation using adaptive meshing. *Turbo Expo Power Land Sea Air. Am. Soc. Mech. Eng.* **2014**, 45738, V05CT16A033.

Disclaimer/Publisher’s Note: The statements, opinions and data contained in all publications are solely those of the individual author(s) and contributor(s) and not of MDPI and/or the editor(s). MDPI and/or the editor(s) disclaim responsibility for any injury to people or property resulting from any ideas, methods, instructions or products referred to in the content.